

Quantum mechanical modeling of the multi-stage Stern–Gerlach experiment conducted by Frisch and Segrè

S. Süleyman Kahraman,^{1,†} Kelvin Titimbo,^{1,†} Zhe He,¹ Jung-Tsung Shen,² and Lihong V. Wang^{1,*}

¹*Caltech Optical Imaging Laboratory, Andrew and Peggy Cherng Department of Medical Engineering, Department of Electrical Engineering, California Institute of Technology, 1200 E. California Blvd., MC 138-78, Pasadena, CA 91125, USA*

²*Department of Electrical and Systems Engineering, Washington University in St. Louis, St. Louis, MO 63130, USA*

(Dated: October 25, 2023)

Multi-stage Stern–Gerlach experiments provide cascaded quantum measurements. The multi-stage Stern–Gerlach experiment conducted by Frisch and Segrè has been modeled analytically using quantum mechanics by Majorana and revised by Rabi by including the hyperfine interaction. However, the theoretical predictions do not match the experimental observation well. Here, we numerically solve the standard quantum mechanical model, via the von Neumann equation, that includes the hyperfine interaction for the time evolution of the spin. Thus far, the coefficients of determination from the standard quantum mechanical model without using free parameters are still below zero, indicating a mismatch between the theory and the experiment. Non-standard variants that improve the match are explored for discussion.

Keywords: spin-flip transitions, electron spin, quantum dynamics, nonadiabatic transitions, hyperfine interaction.

I. INTRODUCTION

The quantum measurement problem tackles the conundrum of wave function collapse, and a quintessential measurement is the Stern–Gerlach (SG) experiment [1–5]. While the single-stage SG experiment was later interpreted as proof of quantization and measurement of the electron spin [6–8], cascaded quantum measurements provide more stringent tests of theories [3, 9, 10]. Frisch and Segrè (FS) conducted the first successful multi-stage SG experiment [1, 10–12] after improving the apparatus from Phipps and Stern [13]. Even though more recent multi-stage SG experiments have been conducted, they differ in the mechanisms of polarizing, flipping, and analyzing spin [14–21]. Most experiments designed for precise atomic measurements use a narrow-band resonant (adiabatic) flipper [14] while the FS experiment uses a wide-band nonadiabatic flipper.

The FS experiment was suggested by Einstein [7, 10, 22] and studied analytically by Majorana [23] and later by Rabi [24]. Majorana investigated the nonadiabatic transition of the electron spin through a closed-form analytical solution, which is now widely used to analyze any two-level system undergoing a nonadiabatic transition [25]. Rabi added the hyperfine interaction to the model but could not obtain an exact closed-form solution similar to the Majorana formula for this multi-level system. With gross approximations, Rabi revised the Majorana formula and still could not predict the experimental observation accurately. Despite additional theoretical studies into similar problems involving multilevel non-

adiabatic transitions [25–31], an accurate solution cannot be obtained when the hyperfine interaction is included.

Among the more recent multi-stage SG experiments [15–20], the study most similar to the FS experiment uses a sequence of coils to obtain the desired magnetic field [15, 16]. The models in these works not only simplified the mathematical description of the magnetic fields generated by the coils but also fit free parameters to predict the experimental observations. We choose to study the FS experiment over other similar experiments because of the simplicity of the nonadiabatic spin flipper, the fully reported experimental parameters required for modeling, and its historical significance.

Here, we numerically simulate the FS experiment using a standard quantum mechanical model using the von Neumann equation without tuning any free parameters and compare the outcome with the predictions by both Majorana and Rabi as well as from an alternative model called co-quantum dynamics (CQD) [32–34]. Even though our approach is a standard method of studying such spin systems, our results do not match with the experimental observations. This discrepancy indicates that either our understanding of the FS experiment is lacking or the standard theoretical model is insufficient. As a natural extension of the SG experiment, the FS experiment holds historical and foundational value for quantum mechanics. We believe it is essential to bring this study to the attention of the research community.

This paper is organized as follows. In Sec. II, we present the experimental configuration used by Frisch and Segrè to measure the fraction of electron spin flip. In Sec. III, we introduce the von Neumann equation and the Hamiltonian for the nuclear-electron spin system. Numerical results for the time evolution of the spins and the final electron spin flip probability are shown here. In Sec. IV, we compare the numerical results with previous

[†] These authors contributed equally.

* Corresponding email:lvw@caltech.edu

solutions. Finally, Sec. V is left for conclusions. Non-standard variants of the quantum mechanical model are explored in the appendices to stimulate discussion.

II. DESCRIPTION OF THE FRISCH–SEGRÈ EXPERIMENT

The schematic used in the Frisch–Segrè experiment [11, 12] is redrawn in Figure 1. There, magnetic regions 1 and 2 act as Stern–Gerlach apparatuses, SG1 and SG2, respectively. In SG1, stable neutral potassium atoms (^{39}K) effused from the oven are spatially separated by the magnetic field gradient according to the orientation of their electron magnetic moment μ_e . The magnetically shielded space containing a current-carrying wire forms the inner rotation (IR) chamber. The shielding reduces the fringe fields from the SG magnets down to the remnant field $B_r = 42 \mu\text{T}$ aligned with $+\hat{z}$. Inside the IR chamber, the current-carrying wire placed at a vertical distance z_a below the atomic beam path creates a cylindrically symmetric magnetic field. The total magnetic field in the IR chamber equals the superposition of the remnant field and the magnetic field created by the electric current I_w flowing through the wire. After SG1, the atoms enter the IR chamber; we approximate the motion to be rectilinear and constant along the y axis. Along the beam path, the magnetic field is given by

$$\mathbf{B}_{\text{exact}} = \frac{\mu_0 I_w z_a}{2\pi(y^2 + z_a^2)} \mathbf{e}_y + \left(B_r - \frac{\mu_0 I_w y}{2\pi(y^2 + z_a^2)} \right) \mathbf{e}_z, \quad (1)$$

where μ_0 is the vacuum permeability; the trajectory of the atom is expressed as $y = vt$, where v is the speed of the atom and the time is set to $t = 0$ at the point on the beam path closest to the wire. The right-handed and unitary vectors $\{\mathbf{e}_x, \mathbf{e}_y, \mathbf{e}_z\}$ describe the directions of the Cartesian system.

The magnetic field inside the IR chamber has a current-dependent null point below the beam path at coordinates $(0, y_{\text{NP}}, -z_a)$, with $y_{\text{NP}} = \mu_0 I_w / 2\pi B_r$. In the vicinity of the null point, the magnetic field components are approximately linear functions of the Cartesian coordinates. Hence, the magnetic field is approximated as a quadrupole magnetic field around the null point [11, 23]. Along the beam path of atoms, the approximate quadrupole field is [32, 34]

$$\mathbf{B}_q = \frac{2\pi B_r^2}{\mu_0 I_w} z_a \mathbf{e}_y + \frac{2\pi B_r^2}{\mu_0 I_w} (y - y_{\text{NP}}) \mathbf{e}_z. \quad (2)$$

For the study of the time evolution of the atom inside the IR chamber both of the fields, $\mathbf{B}_{\text{exact}}$ and \mathbf{B}_q , are considered below.

After the IR chamber, a slit transmits one branch of electron spins polarized by SG1 and blocks the other branch. In the forthcoming theoretical model, we track only the transmitted branch with spin down at the entrance of the IR chamber and ignore the blocked branch.

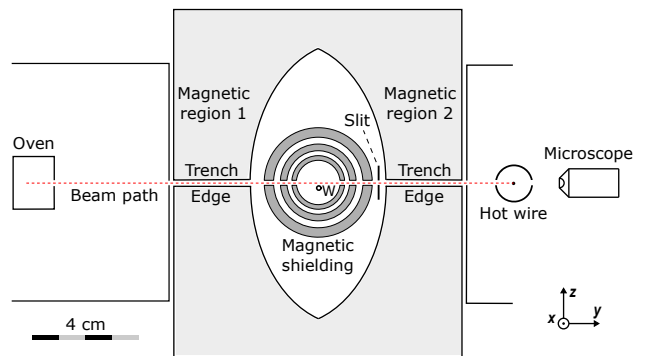


FIG. 1. Redrawn schematic of the original setup [11, 12]. Heated atoms in the oven effuse from a slit. First, the atoms enter magnetic region 1, which acts as SG1. Then, the atoms enter the magnetic shielding (i.e., the IR chamber) containing a current-carrying wire W . Next, a slit selects one branch. Magnetic region 2 acts as SG2. The hot wire is scanned vertically to map the strength of the atomic beam along the z axis. The microscope reads the position of the hot wire.

The atoms that reach SG2 collapse to the eigenstates for the second time and spatially separate owing to the magnetic field gradient. The final distribution of atoms is measured by scanning a hot wire along the z axis while monitored by the microscope. The probability of flip is then measured at different values of the electric current I_w .

III. THEORETICAL DESCRIPTION

The time evolution of the noninteracting atoms in the beam traveling through the IR chamber of the Frisch–Segrè experiment is studied using standard quantum mechanics. We describe the quantum system using the density operator formalism since it embodies the statistical interpretation of quantum mechanics and allows direct simulation of mixed states [35, 36]. The time evolution of the density operator $\hat{\rho}$, specifying the properties of a quantum ensemble of the system, is governed by the von Neumann equation [35, 37, 38]:

$$\frac{\partial \hat{\rho}(t)}{\partial t} = \frac{1}{i\hbar} [\hat{H}(t), \hat{\rho}(t)], \quad (3)$$

where $\hat{H}(t)$ is the Hamiltonian of the system and \hbar is the reduced Plank constant.

Let us consider the quantum system composed of the $4^2\text{S}_{1/2}$ valence electron and the nucleus of the ^{39}K atom. The interaction of the nuclear magnetic moment μ_n and the electron magnetic moment μ_e with an external magnetic field \mathbf{B} is described with the Hamiltonian

$$\hat{H} = \hat{H}_e + \hat{H}_n + \hat{H}_{\text{HFS}}. \quad (4)$$

First, the electron Zeeman term \hat{H}_e describes the interaction between the electron magnetic moment and the

external magnetic field [39] via

$$\hat{H}_e = -\hat{\boldsymbol{\mu}}_e \cdot \mathbf{B}, \quad (5)$$

where $\hat{\boldsymbol{\mu}}_e$ is the quantum operator for $\boldsymbol{\mu}_e$. In ^{39}K atoms, $\hat{\boldsymbol{\mu}}_e$ is only due to the $4s^1$ electron with the spin angular momentum $S = 1/2$ because all other electrons are paired and the net orbital angular momentum is zero. Thus, $\hat{\boldsymbol{\mu}}_e = \gamma_e \hat{\mathbf{S}}$, where $\gamma_e = -1.760\,859\,630\,23(53) \times 10^{11} \text{ rad}/(\text{s T})$ denotes the gyromagnetic ratio of the electron; the electron spin operator $\hat{\mathbf{S}} = \frac{\hbar}{2} \hat{\boldsymbol{\sigma}}$, with the Pauli vector $\hat{\boldsymbol{\sigma}}$ consisting of the Pauli matrices $\{\sigma_x, \sigma_y, \sigma_z\}$. Substitutions yield

$$\hat{H}_e = -\gamma_e \frac{\hbar}{2} \hat{\boldsymbol{\sigma}} \cdot \mathbf{B}. \quad (6)$$

In the 2-dimensional Hilbert space $\mathcal{H}_e = \text{span}(|S, m_s\rangle)$, with $m_s = -S, \dots, S$, the density operator of the electron spin is represented as

$$\hat{\rho}_e = \sum_{m_s, m'_s} \rho_{m_s, m'_s} |S, m_s\rangle \langle S, m'_s|. \quad (7)$$

The nuclear Zeeman Hamiltonian \hat{H}_n describes the interaction of the nuclear magnetic moment with the external magnetic field:

$$\hat{H}_n = -\hat{\boldsymbol{\mu}}_n \cdot \mathbf{B}, \quad (8)$$

where $\hat{\boldsymbol{\mu}}_n = \gamma_n \hat{\mathbf{I}}$ denotes the quantum operator for $\boldsymbol{\mu}_n$, γ_n the nuclear gyromagnetic ratio, and $\hat{\mathbf{I}}$ the nuclear spin quantum operator. For ^{39}K , the nuclear spin $I = 3/2$ and $\gamma_n = 1.250\,061\,2(3) \times 10^7 \text{ rad}/(\text{s T})$ [40]. Therefore, we can write $\hat{\mathbf{I}} = \frac{\hbar}{2} \hat{\boldsymbol{\tau}}$, with $\hat{\boldsymbol{\tau}}$ being the generalized Pauli vector constructed with the generalized Pauli matrices

$$\begin{aligned} \hat{H}_n &= -\gamma_n \frac{\hbar}{2} (B_x \hat{\tau}_x + B_y \hat{\tau}_y + B_z \hat{\tau}_z) \otimes \hat{\sigma}_0 \\ &= -\gamma_n \frac{\hbar}{2} \begin{pmatrix} 3B_z & \sqrt{3}(B_x - iB_y) & 0 & 0 \\ \sqrt{3}(B_x + iB_y) & B_z & 2(B_x - iB_y) & 0 \\ 0 & 2(B_x + iB_y) & -B_z & \sqrt{3}(B_x - iB_y) \\ 0 & 0 & \sqrt{3}(B_x + iB_y) & -3B_z \end{pmatrix} \otimes \hat{\sigma}_0, \quad (13) \end{aligned}$$

$$\hat{H}_{\text{HFS}} = \frac{\pi}{2} \hbar a_{\text{HFS}} (\hat{\tau}_x \otimes \hat{\sigma}_x + \hat{\tau}_y \otimes \hat{\sigma}_x + \hat{\tau}_y \otimes \hat{\sigma}_z) = \frac{\pi}{2} \hbar a_{\text{HFS}} \begin{pmatrix} 3 & 0 & 0 & 0 & 0 & 0 & 0 & 0 \\ 0 & -3 & 2\sqrt{3} & 0 & 0 & 0 & 0 & 0 \\ 0 & 2\sqrt{3} & 1 & 0 & 0 & 0 & 0 & 0 \\ 0 & 0 & 0 & -1 & 4 & 0 & 0 & 0 \\ 0 & 0 & 0 & 4 & -1 & 0 & 0 & 0 \\ 0 & 0 & 0 & 0 & 0 & 1 & 2\sqrt{3} & 0 \\ 0 & 0 & 0 & 0 & 0 & 2\sqrt{3} & -3 & 0 \\ 0 & 0 & 0 & 0 & 0 & 0 & 0 & 3 \end{pmatrix}, \quad (14)$$

for spin $3/2$, namely $\{\tau_x, \tau_y, \tau_z\}$. Substitutions produce

$$\hat{H}_n = -\gamma_n \frac{\hbar}{2} \hat{\boldsymbol{\tau}} \cdot \mathbf{B}. \quad (9)$$

In the 4-dimensional Hilbert space $\mathcal{H}_n = \text{span}(|I, m_I\rangle)$ with $m_I = -I, \dots, I$, the density operator for the nuclear spin is

$$\hat{\rho}_n = \sum_{m_I, m'_I} \rho_{m_I, m'_I} |I, m_I\rangle \langle I, m'_I|. \quad (10)$$

The interaction between the magnetic dipole moments of the nucleus and the electron gives the hyperfine structure (HFS) term \hat{H}_{HFS} . In terms of the electron and nuclear spin operators, the Hamiltonian is written as

$$\hat{H}_{\text{HFS}} = \frac{2\pi a_{\text{HFS}}}{\hbar} \hat{\mathbf{I}} \cdot \hat{\mathbf{S}}, \quad (11)$$

where a_{HFS} reflects the coupling strength. For ^{39}K , a_{HFS} is set to the experimental value $a_{\text{exp}} = 230.859\,860\,1(3) \text{ MHz}$ [40].

Therefore, the 8-dimensional Hilbert space for the combined nuclear–electron spin system is $\mathcal{H} = \mathcal{H}_n \otimes \mathcal{H}_e$. The tensor product combines the bases into the form $|m_I, m_s\rangle$; where for simplicity of notation we have dropped the S and I labels.

The terms of the nuclear–electron spin Hamiltonian $\hat{H} = \hat{H}_e + \hat{H}_n + \hat{H}_{\text{HFS}}$ are expressed as [41, 42]

$$\begin{aligned} \hat{H}_e &= -\gamma_e \frac{\hbar}{2} \hat{\tau}_0 \otimes (B_x \hat{\sigma}_x + B_y \hat{\sigma}_y + B_z \hat{\sigma}_z) \\ &= -\gamma_e \frac{\hbar}{2} \hat{\tau}_0 \otimes \begin{pmatrix} B_z & B_x - iB_y \\ B_x + iB_y & -B_z \end{pmatrix}, \quad (12) \end{aligned}$$

where $\hat{\sigma}_0$ and $\hat{\tau}_0$ are the 2-dimensional and 4-dimensional

identity matrices, respectively. This Hamiltonian has

been validated numerically by comparing the eigenvalues with respect to the external field with the solutions from the Breit–Rabi formula [43].

The overall density operator $\hat{\rho}$ is expressed in the basis $\{|m_I, m_s\rangle\}$ as

$$\hat{\rho} = \sum_{i,j=-I}^I \sum_{k,l=-S}^S \rho_{ik}^{jl} |i, k\rangle\langle j, l|. \quad (15)$$

In the IR chamber, the external magnetic field either in the exact (1) or the quadrupole form (2) is time dependent. An exact closed-form analytical time-dependent solution for the density operator cannot be obtained. For the numerical solution of the time evolution, the von Neumann equation (3) needs to be discretized. We use the second-order Runge–Kutta method as follows [44]:

$$\hat{\rho}(t + \frac{\Delta t}{2}) = \hat{\rho}(t) - \frac{\Delta t}{2} \frac{i}{\hbar} [\hat{H}(t), \hat{\rho}(t)], \quad (16a)$$

$$\hat{\rho}(t + \Delta t) = \hat{\rho}(t) - \Delta t \frac{i}{\hbar} \left[\hat{H}(t + \frac{\Delta t}{2}), \hat{\rho}(t + \frac{\Delta t}{2}) \right], \quad (16b)$$

where Δt is the temporal step size. We have solved the same equations using various other algorithms written in Julia [45].

In order to solve the initial value problem, we first define the initial density operator $\hat{\rho}(t_0)$ at time t_0 , corresponding to the entrance of the IR chamber. Since we track the branch with electron spin down (i.e., $|m_s = -1/2\rangle$) and $\langle \hat{S}_z \rangle = -\hbar/2$, the initial state for the electronic component is

$$\hat{\rho}_e(t_0) = \hat{\rho}_{\text{exact}}(t_0) = |-1/2\rangle\langle -1/2| = \begin{pmatrix} 0 & 0 \\ 0 & 1 \end{pmatrix}. \quad (17)$$

The electron spin flips adiabatically near the wire [11, 34] to spin up, yielding $\langle \hat{S}_z \rangle = \hbar/2$. Thereafter, we numerically track the non-adiabatic flip due to the null point by considering the quadrupole approximation \mathbf{B}_q shown in (2). Thus, we reset the initial state to [23, 32, 34]

$$\hat{\rho}_e(t_0) = \hat{\rho}_{\text{quad}}(t_0) = |+1/2\rangle\langle +1/2| = \begin{pmatrix} 1 & 0 \\ 0 & 0 \end{pmatrix}. \quad (18)$$

In contrast, the initial nuclear state is assumed to be maximally mixed [24]:

$$\hat{\rho}_n(t_0) = \frac{1}{4} \begin{pmatrix} 1 & 0 & 0 & 0 \\ 0 & 1 & 0 & 0 \\ 0 & 0 & 1 & 0 \\ 0 & 0 & 0 & 1 \end{pmatrix}. \quad (19)$$

Then, the initial density operator of the combined system is assumed to be factorized as $\hat{\rho}(t_0) = \hat{\rho}_n(t_0) \otimes \hat{\rho}_e(t_0)$.

Finally, we calculate the expectations of spin measurements, for the electron and the nucleus, in the z direction as

$$\langle \hat{S}_z \rangle = \frac{\hbar}{2} \langle \hat{\sigma}_z \rangle = \frac{\hbar}{2} \text{Tr}(\hat{\rho}(t) \hat{\sigma}_z), \quad (20a)$$

$$\langle \hat{I}_z \rangle = \frac{\hbar}{2} \langle \hat{\tau}_z \rangle = \frac{\hbar}{2} \text{Tr}(\hat{\rho}(t) \hat{\tau}_z), \quad (20b)$$

where Tr denotes the trace.

For the computation of the electron spin flip probability, let us introduce the projector operators $M_+ = |+1/2\rangle\langle +1/2|$ and $M_- = |-1/2\rangle\langle -1/2|$, such that they are orthogonal and span the Hilbert space for the electron spin \mathcal{H}_e . The operators M_+ and M_- correspond to projective measurements of electron spin $+\hbar/2$ and $-\hbar/2$, respectively. The flip probability of spin after exiting the IR chamber at time t_f is

$$p = \text{Tr}(\hat{\rho}(t_f) M_+). \quad (21)$$

A. Excluding hyperfine interaction

We first consider the case $\hat{H} = \hat{H}_e$ by neglecting the nuclear component. The analytical asymptotic solution for this model was found using the quadrupole field approximation by Majorana [23] and applied to the Frisch–Segré experiment [11]. Here, a numerical solution is provided for both the exact and quadrupole fields.

Figure 2a shows the evolution of $\langle \hat{S}_z \rangle$ over the flight of the atom in the IR chamber. The expectation towards the end of the IR chamber oscillates with time. As the magnetic field strength increases, the oscillation decays. Hence, we average the expectation over the final one-eighth of the flight before the exit of the IR chamber.

Figure 2b shows the flip probability of the electron spin observed in SG2 as spin up, computed using (21), for the exact and quadrupole fields at different wire currents. The numerical prediction using the quadrupole approximation agrees exactly with Majorana’s analytical prediction [23] and closely with the numerical prediction using the exact field. The coefficients of determination R^2 between the numerical predictions and the experimental data are, however, -18.9 and -19.9 for the exact and quadrupole fields, respectively. Therefore, this model does not predict the experimental observation well.

B. Including hyperfine interaction

We now consider \hat{H} as in (4) by including the hyperfine interaction. This model is implemented similarly as above. Figure 3a illustrates $\langle \hat{S}_z \rangle$ and $\langle \hat{I}_z \rangle$ versus the flight time of the atoms in the IR chamber for the exact field at $I_w = 0.1$ A.

Figure 3b shows the flip probabilities predicted by the numerical solution in comparison to Rabi’s analytical solution [24] and the experimental observation [11]. The coefficients of determination R^2 of our model for the exact and quadrupole fields in relation to the experimental observation are -11.43 and -16.27 , respectively; Rabi’s prediction has an $R^2 = -0.02$. Clearly, our standard quantum mechanical model or Rabi’s solution, even if

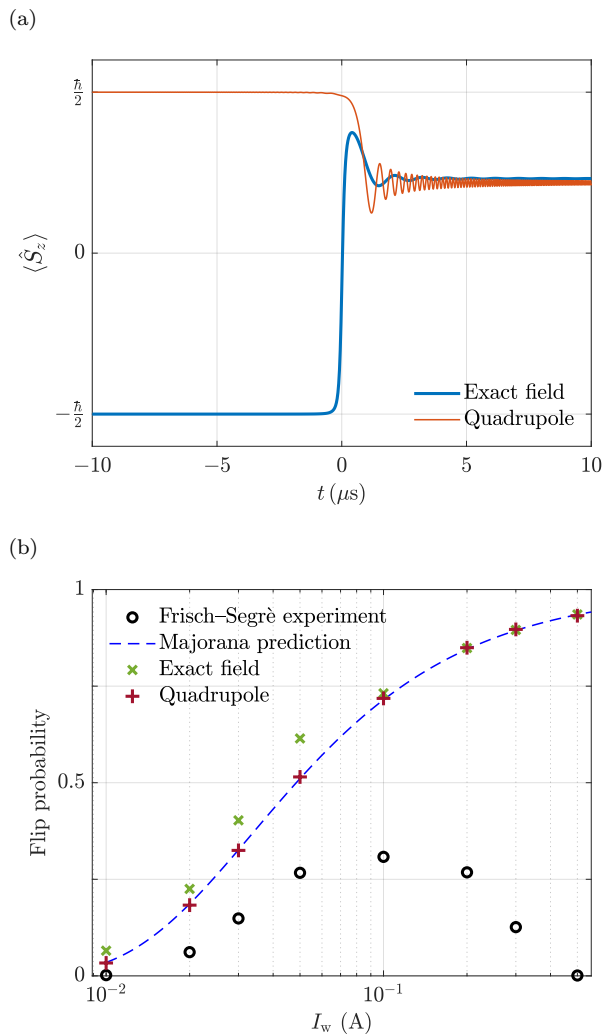


FIG. 2. (a) Time evolution of $\langle \hat{S}_z \rangle$ for the exact and quadrupole fields at wire current $I_w = 0.1$ A. (b) Flip probability of the electron spin versus the wire current. The numerical simulations match with Majorana’s prediction [23] but not with the experimental observation [11].

the HFS is considered, does not predict the experimental observation well.

IV. DISCUSSION

In the main text, we have only considered a maximally mixed initial nuclear state as in (19), which is common in the literature [24], and have used only the experimentally measured value of a_{exp} . In the appendices, we have considered various other initial states (see Appendix A) and other hyperfine interaction strengths (see Appendix B). Among all the cases, the best match with the experimental observation has $R^2 = 0.51$ (see Appendix C and Table I). We have also tried to match the observations using only the electron spin without hyperfine coupling and treating the remnant field as a free parameter with-

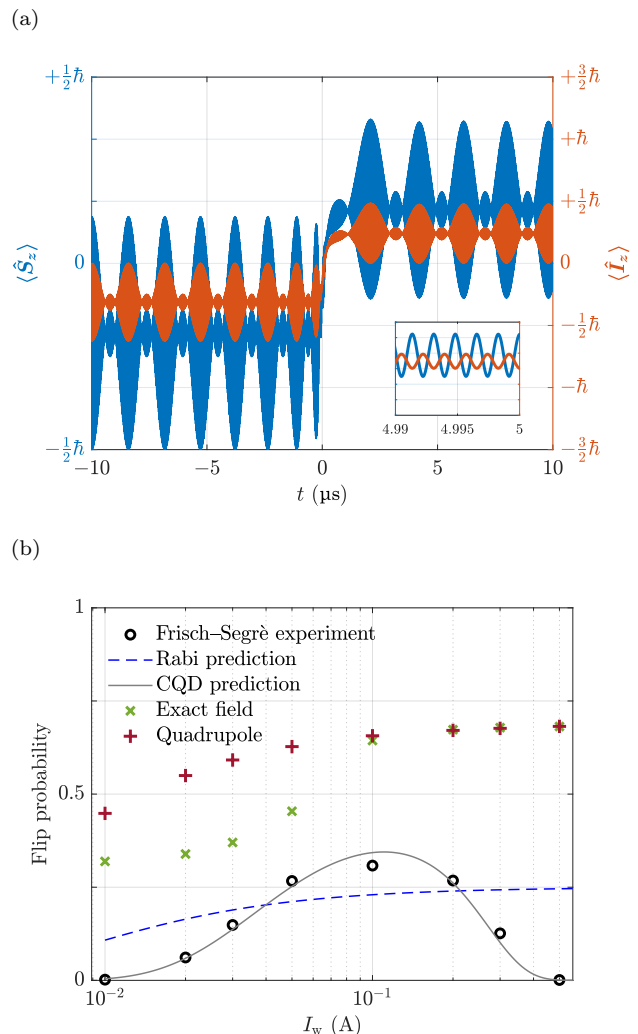


FIG. 3. (a) Evolution of $\langle \hat{S}_z \rangle$ and $\langle \hat{I}_z \rangle$ for the exact field over the flight duration within the IR chamber at $I_w = 0.1$ A. (b) Flip probability of the electron spin for the exact and quadrupole fields when the hyperfine interaction is included. The numerical predictions do not match with the experimental observation nor with Rabi’s and CQD’s predictions [24, 32].

out any justification (see Appendix E).

While one might question inaccuracies in the experiment conducted in the 1930s, a possible reason for the discrepancy is the deficiency of the models. The deficiency of Majorana’s prediction is likely due to the lack of hyperfine interaction, and the deficiency of Rabi’s prediction might be caused by the approximations made during the modification to the Majorana formula. Without such approximations, our numerical model that follows the standard quantum mechanical formalism should reach a higher coefficient of determination ($R^2 \sim 1$) but still does not accurately match the experimental observation. Surprisingly, recent “semi-classical” studies under CQD [32–34] have been able to match the Frisch–Segrè experimental observation well both analytically and nu-

merically without using free parameters.

The full Hamiltonian, including the hyperfine interaction term first written by Fermi [46], cannot predict the experimental observations. The standard hyperfine treatment uses the value of a_{exp} measured in spectroscopic experiments [14, 40] but does not predict the FS observation. Much closer matches can be obtained if a_{HFS} is reduced by orders of magnitude. These smaller values are more consistent with the Fermi contact interaction [46, 47]. However, the Fermi contact interaction cannot accurately predict magnetic resonance-based experiments for any atoms other than hydrogen or its isotopes [14, 40, 47]. This discrepancy might be due to the ill-defined nature of the Fermi contact interaction [48]. For any atom, the mathematical structure of the interaction term is well-studied [49, 50], but the exact values of the coefficients are still experimentally measured [14, 40]. Most of the precise measurements of a_{exp} are resonance-based at optical or radio frequencies, whereas the FS experiment uses nonadiabatic transitions. One questions whether the model of the FS experiment could benefit from an improved Hamiltonian.

V. CONCLUSIONS

Simulating the FS experiment [11, 12] using a standard quantum mechanical model has yielded the following conclusions:

- The FS observations cannot be replicated by modeling only the electron spin without hyperfine coupling (Section III A). Altering the reported experimental parameters without appropriate justifications improves the prediction (Appendix E).
- The FS observations cannot be replicated by modeling the atom as a pair of electron and nuclear spins if the hyperfine interaction coefficient is set to the experimental a_{exp} and the initial nuclear state is maximally mixed (Section III B).
- The FS observations can be modeled with an R^2 of approximately 0.5 if the hyperfine coefficient a_{HFS} and the initial nuclear state are allowed to vary (Appendix C). However, the value of a_{HFS} is lowered by a few orders of magnitude from a_{exp} to be closer to the theoretical Fermi contact prediction. Furthermore, because SG1 creates only two instead of eight $((2I+1)(2S+1) = 8)$ discernible branches, the initial nuclear state is not measured directly and thus may not have been chosen correctly.

Based on some of the non-standard cases that can improve the model prediction of the FS observation (see Appendices), one might question the following:

- What is the nuclear spin state before and after each SG apparatus? How does the nuclear spin state affect the electron spin flip?

- Is the hyperfine structure coefficient measured via narrow-band (adiabatic) resonant experiments appropriate for wide-band nonadiabatic experiments like the FS experiment?
- Do we need a more sophisticated model of the atom (especially, the nucleus) to understand and predict the SG and nonadiabatic experiments?
- Do the SG apparatuses in the FS experiment truly follow the Born principle? Is there a (hidden) variable, such as the nuclear spin, affecting the FS measurement (see Appendix D)?

Even though we think we understand multi-stage SG experiments, detailed modeling fails to explain the observations of the first of such experiments [11, 12]. Later multi-stage SG experiments include different designs of the SG apparatuses and spin flippers, and the associated models use free parameters for fitting [15–20]. Given the foundational importance of the multi-stage SG experiments as cascaded quantum measurements, we believe that the mismatch between the theory and the experiment here merits further investigation.

ACKNOWLEDGMENTS

We thank Xukun Lin for scrutinizing the source codes. This project has been made possible in part by grant number 2020-225832 from the Chan Zuckerberg Initiative DAF, an advised fund of the Silicon Valley Community Foundation.

SUPPLEMENTAL MATERIAL

Our source codes are available online [51].

Appendix A: Modified initial states

A recently developed theory called CQD [32] matches the experiment well [11] and yields an anisotropic distribution for the nuclear spin after SG1. Inspired by this work, we explore various initial states for the nuclear spin in addition to the maximally mixed state. We consider pure nuclear initial states

$$|\Psi_n\rangle = c_1 |+3/2\rangle + c_2 |+1/2\rangle + c_3 |-1/2\rangle + c_4 |-3/2\rangle, \quad (\text{A1})$$

where for simplicity we constrain $c_i \in \mathbb{R}$, for $i = 1, \dots, 4$. Then, the initial state of the compound nuclear–electron spin system is

$$\hat{\rho}_{\text{pure}} = |\Psi_n\rangle\langle\Psi_n| \otimes \hat{\rho}_e(t_0). \quad (\text{A2})$$

Also, we consider a family of mixed nuclear initial states with all off-diagonal elements set to zero. Thus, the initial state for the compound system reads

$$\hat{\rho}_{\text{mixed}} = \begin{pmatrix} d_1 & 0 & 0 & 0 \\ 0 & d_2 & 0 & 0 \\ 0 & 0 & d_3 & 0 \\ 0 & 0 & 0 & d_4 \end{pmatrix} \otimes \hat{\rho}_e(t_0). \quad (\text{A3})$$

Some of the tested pure states include $(c_1, c_2, c_3, c_4) \propto (1, 1, 1, 1)$, $(0, 1, 2, 3)$, $(1, 0, 0, 1)$, $(1, 0, 0, \sqrt{2})$, and $(1, 0, 0, \sqrt{3})$. Meanwhile, some of the tried mixed states include $(d_1, d_2, d_3, d_4) \propto (1, 1, 1, 1)$, $(0, 1, 2, 3)$, $(1, 0, 0, 1)$, $(1, 0, 0, 2)$, and $(1, 0, 0, 3)$.

Appendix B: Modified HFS coefficients

Up to now, we have used the experimentally measured HFS coefficient value, $a_{\text{exp}} = 230.859\,860\,1(3)$ MHz [40], which does not accurately predict the experimental observation by Frisch and Segrè. Here, we modify the hyperfine coefficient to improve the match.

One way to calculate the HFS coefficient is to use the Fermi contact interaction as follows [39, 41, 46, 52]:

$$2\pi\hbar a_{\text{HFS}} = -\hbar^2 \frac{2\mu_0}{3} \gamma_e \gamma_n |\psi(0)|^2, \quad (\text{B1})$$

where $\psi(\mathbf{r})$ denotes the spatial wave function of the electron. The wave function for the $4s^1$ electron in ^{39}K does not have an exact solution. However, various approximations are available [32, 53, 54], yielding the following HFS coefficients:

$$a_1 = -\hbar \frac{\mu_0 \gamma_e \gamma_n}{4\pi^2 R^3} \approx 355 \text{ kHz}, \quad (\text{B2a})$$

$$a_2 = -\hbar \frac{8\mu_0 \gamma_e \gamma_n}{3\pi^4 R^3} \approx 384 \text{ kHz}, \quad (\text{B2b})$$

$$a_3 = -\hbar \frac{28.4\mu_0 \gamma_e \gamma_n}{6\pi^2 R^3} \approx 6.72 \text{ MHz}, \quad (\text{B2c})$$

where $R = 275$ pm is the van der Waals radius for ^{39}K . Another set of values for a_{HFS} are obtained on the basis of an alternative averaging method [32]:

$$a_4 = -\hbar \frac{5\mu_0 \gamma_e \gamma_n}{32\pi^2 R^3} \approx 222 \text{ kHz}, \quad (\text{B3a})$$

$$a_5 = -\hbar \frac{2\mu_0 \gamma_e \gamma_n}{3\pi^4 R^3} \approx 95.9 \text{ kHz}, \quad (\text{B3b})$$

$$a_6 = -\hbar \frac{0.138\mu_0 \gamma_e \gamma_n}{2\pi^2 R^3} \approx 98.0 \text{ kHz}. \quad (\text{B3c})$$

All of these values along with the experimental value, a_{exp} , have been tried.

Appendix C: Selected outcomes

Table I and Figure 4 show the matches with the highest R^2 among the tested cases. Among all the initial density

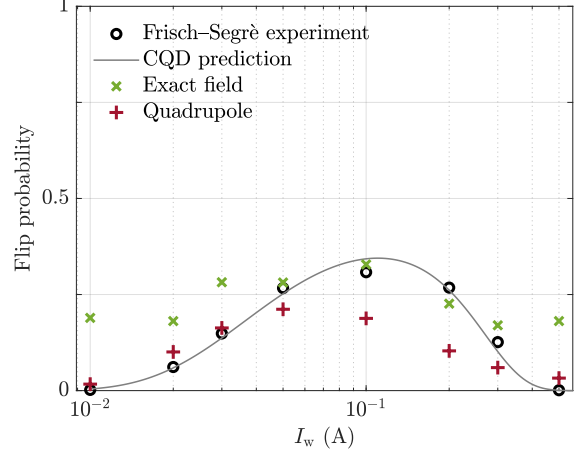


FIG. 4. Flip probability of the electron spin versus the wire current for both the exact and quadrupole fields. Only the best matches of the theoretical predictions with the experimental observation are plotted, and the corresponding parameters are included in Table I.

matrices and the HFS coefficients considered, the combination of the maximally distributed pure initial nuclear state and a_2 matches the experiment the closest under the exact field. Under the quadrupole field, the closest match is from the combination of the anisotropic pure initial nuclear state and a_4 .

Ideally, one should sample all feasible density matrices for a 4-state spin system and try each case with experimental and theoretical HFS coefficients along with other possible values. However, even if the Frisch–Segrè data can be matched for a specific initial state, one should still explain how such a state can be obtained through SG1. The cases considered in this paper are the simplest cases one might think of, and the results do not match well with the experimental observation.

Appendix D: Deviation from the Born principle

Recent theoretical studies that use CQD [32, 33] have predicted the Frisch–Segrè experimental observation with high coefficients of determination. Within the framework of CQD, the continuous distribution of nuclear spins after the first Stern–Gerlach stage becomes anisotropic (heart-shaped), leading to deviation from the Born principle [32]; as a result, the probability of flip becomes $p = (\text{Tr}(\rho(t_f)M_+))^2$. Here, we translate the anisotropic distribution to

$$\hat{\rho}_n(t_0) = \frac{1}{3} \begin{pmatrix} 1 & 0 & 0 & 0 \\ 0 & 0 & 0 & 0 \\ 0 & 0 & 0 & 0 \\ 0 & 0 & 0 & 2 \end{pmatrix}. \quad (\text{D1})$$

Further, we use a_4 to be consistent with CQD and include a_{exp} for comparison. The numerical outcome matches the experimental observation well, yielding coefficients of determination of $R^2 = 0.61$ for the exact field and

TABLE I. Coefficients of determination (R^2) for the flip probabilities with respect to the experimental observation for various HFS coefficients.

Initial state	Magnetic field	a_{exp}	a_2	a_4
$\hat{\rho}_n(t_0) = \frac{1}{4} \begin{pmatrix} 1 & 0 & 0 & 0 \\ 0 & 1 & 0 & 0 \\ 0 & 0 & 1 & 0 \\ 0 & 0 & 0 & 1 \end{pmatrix}$	exact	-11.43	-2.47	-2.54
	quadrupole	-16.27	-0.55	-1.41
$ \Psi_n(t_0)\rangle = \frac{1}{2}(+3/2\rangle + +1/2\rangle + -1/2\rangle + -3/2\rangle)$	exact	-11.58	0.01	-5.99
	quadrupole	-16.70	-0.20	0.01
$ \Psi_n(t_0)\rangle = \frac{1}{\sqrt{14}}(0 +3/2\rangle + 1 +1/2\rangle + 2 -1/2\rangle + 3 -3/2\rangle)$	exact	-16.74	-0.76	-4.38
	quadrupole	-9.78	-0.54	0.51

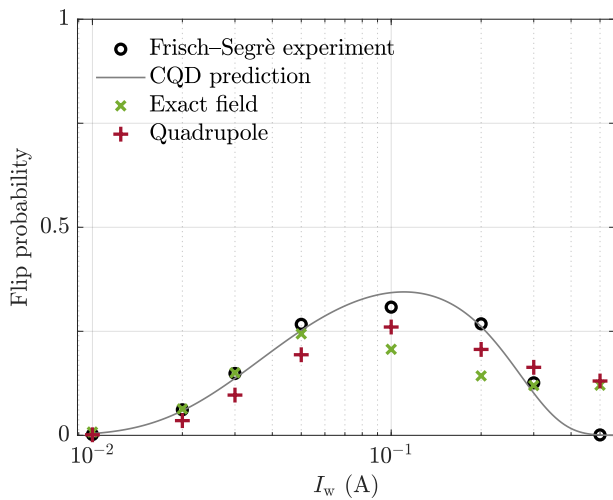


FIG. 5. Squared flip probability of the electron spin versus the wire current for both the exact and quadrupole fields. Only the theoretical predictions using a_4 are plotted, and the corresponding R^2 values are listed in Table II.

TABLE II. Coefficients of determination (R^2) for the artificially squared flip probabilities with respect to the experimental observation for two different HFS coefficients.

Initial state	Magnetic field	a_{exp}	a_4
$\hat{\rho}_n(t_0) = \frac{1}{3} \begin{pmatrix} 1 & 0 & 0 & 0 \\ 0 & 0 & 0 & 0 \\ 0 & 0 & 0 & 0 \\ 0 & 0 & 0 & 2 \end{pmatrix}$	exact	-10.81	0.61
	quadrupole	-6.34	0.69

$R^2 = 0.69$ for the quadrupole approximation, as shown in Table II and Figure 5. Although this modification is not justified under quantum mechanics, we report the result to stimulate discussion.

Appendix E: Fitting for the remnant field

The remnant field near the null point is clearly reported to be $B_r = 42 \mu\text{T}$ aligned with $+\hat{z}$. If we allow this remnant field to be a three-dimensional fitting vector $\mathbf{B}_{\text{fit}} = (B_x, B_y, B_z)$, it is possible to improve the model prediction of the FS experimental observation. Since there is no exact closed-form solution if hyperfine interaction is included, it is not straightforward to fit for the remnant field. However, without hyperfine interaction, the eight-level system is reduced to two levels, leading to an exact closed-form solution similar to the Zener solution [25, 55–57]. The 2D null point where only the y and z components of the field vanish is located at the coordinates of

$$(0, y'_{\text{NP}}, z'_{\text{NP}}) = \left(0, \frac{\mu_0 I_w B_z}{2\pi(B_y^2 + B_z^2)}, -z_a - \frac{\mu_0 I_w B_y}{2\pi(B_y^2 + B_z^2)}\right). \quad (\text{E1})$$

The field can be approximated around this null point to the first order as

$$\mathbf{B}_{\text{q,fit}} = B_x \mathbf{e}_x + \left(\frac{4\pi B_y B_z}{\mu_0 I_w} (y - y'_{\text{NP}}) - \frac{2\pi(B_z^2 - B_y^2)}{\mu_0 I_w} z'_{\text{NP}} \right) \mathbf{e}_y + \left(-\frac{2\pi(B_z^2 - B_y^2)}{\mu_0 I_w} (y - y'_{\text{NP}}) - \frac{4\pi B_y B_z}{\mu_0 I_w} z'_{\text{NP}} \right) \mathbf{e}_z. \quad (\text{E2})$$

Using the new approximated field, $\mathbf{B}_{\text{q,fit}}$, the Hamiltonian has the structure of

$$\hat{H}_{\text{fit}}(t) = -\gamma_e \frac{\hbar}{2} \mathbf{B}_{\text{q,fit}} \cdot \hat{\boldsymbol{\sigma}} = \begin{pmatrix} c_0 + c_1 t & a_0 - i(b_0 + b_1 t) \\ a_0 + i(b_0 + b_1 t) & -(c_0 + c_1 t) \end{pmatrix} = -\gamma_e \frac{\hbar}{2} \begin{pmatrix} -B_z - \frac{4\pi B_y B_z z_a}{\mu_0 I_w} - \frac{2\pi v(B_y^2 - B_z^2)}{\mu_0 I_w} t & B_x - i \left(-\frac{2\pi(2B_y B_z y'_{\text{NP}} + (B_y^2 - B_z^2) z'_{\text{NP}})}{\mu_0 I_w} + \frac{4\pi v B_y B_z t}{\mu_0 I_w} \right) \\ B_x + i \left(-\frac{2\pi(2B_y B_z y'_{\text{NP}} + (B_y^2 - B_z^2) z'_{\text{NP}})}{\mu_0 I_w} + \frac{4\pi v B_y B_z t}{\mu_0 I_w} \right) & B_z + \frac{4\pi B_y B_z z_a}{\mu_0 I_w} + \frac{2\pi v(B_y^2 - B_z^2)}{\mu_0 I_w} t \end{pmatrix}, \quad (\text{E3})$$

where we have replaced $y = vt$ to obtain the time dependence. To transform into Zener's formulation, we need to rotate the coordinate system. Let us first rotate around \mathbf{e}_x by θ_x using a matrix of $\hat{R}_x = e^{-i\hat{\sigma}_x \theta_x/2}$. This rotation moves all of the time dependence into the diagonal terms. Then, we can rotate around \mathbf{e}_z by θ_z using a matrix of $\hat{R}_z = e^{-i\hat{\sigma}_z \theta_z/2}$. The final rotated Hamiltonian can be calculated as $\hat{H}_{\text{rot}}(t) = \hat{R}_z \hat{R}_x \hat{H}_{\text{fit}}(t) \hat{R}_x^\dagger \hat{R}_z^\dagger$. Now, we still need to shift the time coordinate to avoid time-invariant diagonal terms. For this purpose, let us define a new variable $t' = t + t_s$. The rotated and shifted wavefunction and Hamiltonian are given as

$$\hat{H}_{\text{rot}}(t') = \hat{R}_z \hat{R}_x \hat{H}_{\text{fit}}(t' - t_s) \hat{R}_x^\dagger \hat{R}_z^\dagger = \begin{pmatrix} -\frac{\nu}{2} t' & -\frac{\Delta}{2} \\ -\frac{\Delta}{2} & \frac{\nu}{2} t' \end{pmatrix}, \quad (\text{E4})$$

where

$$\theta_x = \arctan\left(\frac{b_1}{c_1}\right), \quad (\text{E5a})$$

$$\theta_z = \arctan\left(\frac{b_1 c_0 - b_0 c_1}{a_0 \sqrt{b_1^2 + c_1^2}}\right), \quad (\text{E5b})$$

$$t_s = \frac{b_0 b_1 + c_0 c_1}{b_1^2 + c_1^2}, \quad (\text{E5c})$$

$$\nu = -2\sqrt{b_1^2 + c_1^2}, \quad (\text{E5d})$$

$$\Delta = -2\sqrt{a_0^2 + \frac{(b_1 c_0 - b_0 c_1)^2}{b_1^2 + c_1^2}}. \quad (\text{E5e})$$

The solutions to the rotated and shifted system can be given by the parabolic cylinder functions using Zener's solution. The initial state has to be given in the same rotated and shifted system.

$$\begin{aligned} |\Psi_{\text{rot}}(z)\rangle &= \hat{U}_{\text{rot}}(z, z_0) |\Psi_{\text{rot}}(z_0)\rangle \\ &= \begin{pmatrix} c_1 D_{-i\delta-1}(z) + c_2 D_{i\delta}(iz) \\ e^{-i\pi/4} \left(c_2 \sqrt{\delta} D_{i\delta-1}(iz) + c_1 \frac{1}{\sqrt{\delta}} D_{-i\delta}(z) \right) \end{pmatrix}, \quad (\text{E6}) \end{aligned}$$

where each element of the operator $\hat{U}_{\text{rot}}(z, z_0)$ is

$$\hat{U}_{\text{rot}}^{1,1}(z, z_0) = \frac{\Gamma(i\delta + 1)}{\sqrt{2\pi}} (D_{-i\delta-1}(z) D_{-i\delta}(-z_0) + D_{-i\delta-1}(-z) D_{-i\delta}(z_0)), \quad (\text{E7a})$$

$$\hat{U}_{\text{rot}}^{1,2}(z, z_0) = \frac{\Gamma(i\delta + 1)}{\sqrt{2\pi}} \frac{\sqrt{\delta}}{e^{-i\pi/4}} (D_{-i\delta-1}(-z) D_{-i\delta-1}(z_0) - D_{-i\delta-1}(z) D_{-i\delta-1}(-z_0)), \quad (\text{E7b})$$

$$\hat{U}_{\text{rot}}^{2,1}(z, z_0) = \frac{\Gamma(i\delta + 1)}{\sqrt{2\pi}} \frac{e^{-i\pi/4}}{\sqrt{\delta}} (D_{-i\delta}(-z) D_{-i\delta}(z_0) - D_{-i\delta}(z) D_{-i\delta}(-z_0)), \quad (\text{E7c})$$

$$\hat{U}_{\text{rot}}^{2,2}(z, z_0) = \frac{\Gamma(i\delta + 1)}{\sqrt{2\pi}} (D_{-i\delta}(-z) D_{-i\delta-1}(z_0) + D_{-i\delta}(z) D_{-i\delta-1}(-z_0)), \quad (\text{E7d})$$

with

$$z = e^{i\pi/4} \sqrt{\frac{\nu}{\hbar}} t', \quad (\text{E8a})$$

$$z_0 = e^{i\pi/4} \sqrt{\frac{\nu}{\hbar}} t'_0, \quad (\text{E8b})$$

$$\delta = \frac{\Delta^2}{4\nu\hbar}, \quad (\text{E8c})$$

$$|\Psi_{\text{rot}}(z)\rangle = \hat{R}_z \hat{R}_x |\Psi(t)\rangle. \quad (\text{E8d})$$

Hence,

$$|\Psi(t)\rangle = \hat{U} |\Psi(t_0)\rangle = \hat{R}_z^\dagger \hat{R}_x^\dagger \hat{U}_{\text{rot}} \hat{R}_x \hat{R}_z |\Psi(t_0)\rangle. \quad (\text{E9})$$

Using the exact solution above, one can fit for the field, yielding $\mathbf{B}_{\text{fit}} = (10, 5.14, 41.87) \mu\text{T}$. The coefficient of determination with this remnant field is $R^2 = 0.86$ (0.35) for the quadrupole (exact) field. The additional weak remnant field orthogonal to the reported remnant field would improve the model prediction. Unfortunately, the

hyperfine interaction is unrealistically neglected.

The full hyperfine system cannot be analytically solved. Instead, using the fitting results from above, we obtain a much lower coefficient of determination, $R^2 = -10.97(-7.91)$ for the quadrupole (exact) field. One can exhaustively fit for the field, which is however computationally expensive. Importantly, such fitting simply ignores the reported experimental parameters in the original paper[11, 12].

In order to further simplify the expression for the final flip probability, it is possible to assume that the region of interaction is infinitely long (i.e., $-t_0 = t_f$ and $t_f \rightarrow \infty$). In this limit, the operator $\hat{U}_{\text{rot}}(z, z_0)$ can be written as

$$\lim_{\substack{t_0 \rightarrow -\infty \\ t_f \rightarrow \infty}} \hat{U}_{\text{rot}}(z_f, z_0) = \begin{pmatrix} T & R e^{-i\theta_t} \\ -R e^{i\theta_t} & T \end{pmatrix}, \quad (\text{E10})$$

where

$$T = e^{-\pi\delta}, \quad (\text{E11a})$$

$$R = \sqrt{1 - e^{-2\pi\delta}}, \quad (\text{E11b})$$

$$\theta_t = \frac{\pi}{4} + \text{Arg}(\Gamma(1 - i\delta)) + (t + t_s)^2 \frac{\nu}{2\hbar} + 2\delta \ln \left((t + t_s) \sqrt{\frac{\nu}{\hbar}} \right). \quad (\text{E11c})$$

The limit of the evolution operator in the original frame is

$$\lim_{\substack{t_0 \rightarrow -\infty \\ t_f \rightarrow \infty}} \hat{U} = \lim_{\substack{t_0 \rightarrow -\infty \\ t_f \rightarrow \infty}} \left(\hat{R}_z^\dagger \hat{R}_x^\dagger \hat{U}_{\text{rot}} \hat{R}_x \hat{R}_z \right) = \begin{pmatrix} T - iR \cos \theta_t \sin \theta_x & e^{i\theta_z} R (\cos \theta_t \cos \theta_x - i \sin \theta_t) \\ -e^{-i\theta_z} R (\cos \theta_t \cos \theta_x + i \sin \theta_t) & T + iR \cos \theta_t \sin \theta_x \end{pmatrix}. \quad (\text{E12})$$

The final probability measured in the experiment can be obtained from the upper-left diagonal element of this matrix as

$$p_{\text{flip}} = T^2 + R^2 \sin^2 \theta_x \cos^2 \theta_t = e^{-2\pi\delta} + (1 - e^{-2\pi\delta}) \left(\frac{2B_y B_z}{B_y^2 + B_z^2} \right)^2 \cos^2 \theta_t. \quad (\text{E13})$$

The final probability p_{flip} has a rapidly oscillating term due to $\cos^2 \theta_t$. The physical reason for the oscillation can be attributed to the precession along the tuned remnant field direction. Furthermore, the oscillating term is sensitive to experimental parameters, such as the speed of the atom. Hence, the final flip probability is not slowly varying if the uniform remnant field has an arbitrary direction. In a more realistic model, the field in the IR chamber would smoothly change into the field generated by the SG apparatuses.

Nevertheless, p_{flip} can be used to find a lower and upper bound since $|\cos^2 \theta_t| \leq 1$. The equation can also be used to average over a range of experimental parameters describing the molecular beam. Here, we simply

set $-t_0 = t_f = 11 \mu\text{s}$ as in the previous sections and fit the FS data, yielding $\mathbf{B}_{\text{fit}} = (10, 6.41, 41.63) \mu\text{T}$. The coefficient of determination with this remnant field is $R^2 = 0.79(0.40)$ for the quadrupole (exact) field. With hyperfine interaction added, the same field yields a coefficient of determination of $R^2 = -7.91(-10.17)$ for the quadrupole (exact) field.

While the algorithm for the fitting procedure can be more optimal and the model for the arbitrary field direction can be more sophisticated, an additional remnant field was not reported. Hence, even if a close match can be obtained, it will not be modeling the reported original experiment.

-
- [1] W. Gerlach and O. Stern, Der experimentelle nachweis des magnetischen moments des silberatoms, *Z. Phys.* **8**, 110 (1922).
 - [2] W. Gerlach and O. Stern, Über die richtungsquantelung im magnetfeld, *Ann. Phys.* **379**, 673 (1924).
 - [3] J. J. Sakurai and J. Napolitano, *Modern Quantum Mechanics*, 2nd ed. (Addison-Wesley, 2011).
 - [4] R. P. Feynman, R. B. Leighton, and M. L. Sands, *The Feynman Lectures on Physics*, Vol. III: Quantum Mechanics (Basic Books, 2011).

-
- [5] A. Messiah, *Quantum Mechanics* (Dover Publications, Inc, 2020).
 - [6] G. Uhlenbeck and S. Goudsmit, Ersetzung der hypothese vom unmechanischen zwang durch eine forderung bezüglich des inneren verhaltens jedes einzelnen elektrons, *Naturwissenschaften* **13**, 953 (1925).
 - [7] H. Schmidt-Böcking, L. Schmidt, H. J. Lüdde, W. Trageser, A. Templeton, and T. Sauer, The Stern–Gerlach experiment revisited, *Eur. Phys. J. H* **41**, 327 (2016).
 - [8] D. Castelvechi, The Stern–Gerlach experiment at 100,

- Nat. Rev. Phys. **4**, 140 (2022).
- [9] W. Heisenberg, Über den anschaulichen inhalt der quantentheoretischen kinematik und mechanik, *Z. Phys.* **43**, 172 (1927).
- [10] B. Friedrich and H. Schmidt-Böcking, eds., *Molecular Beams in Physics and Chemistry: From Otto Stern's Pioneering Exploits to Present-Day Feats* (Springer, 2021).
- [11] R. Frisch and E. Segrè, Über die einstellung der richtungsquantelung. II, *Z. Phys.* **80**, 610 (1933).
- [12] R. Frisch and E. Segrè, Ricerche Sulla Quantizzazione Spaziale, *Il Nuovo Cimento* **10**, 78 (1933).
- [13] T. E. Phipps and O. Stern, Über die Einstellung der Richtungsquantelung, *Zeitschrift für Physik* **73**, 185 (1932).
- [14] N. Ramsey, *Molecular beams.*, The International series of monographs on physics (Clarendon Press, 1956).
- [15] W. Schroder and G. Baum, A spin flipper for reversal of polarisation in a thermal atomic beam, *Journal of Physics E: Scientific Instruments* **16**, 52 (1983).
- [16] W. Schroder, *Measurement of spin-dependent asymmetries in inelastic collisions of electrons with light alkali atoms*, Ph.D. thesis (1982).
- [17] R. D. Hight and R. T. Robiscoe, Nonadiabatic transition in $n=2$ atomic hydrogen, *Physical Review A* **17**, 561 (1978).
- [18] D. Hight, *Non-adiabatic spin transitions in metastable hydrogen*, Ph.D. thesis (1975).
- [19] Y. Margalit, O. Dobkowski, Z. Zhou, O. Amit, Y. Japha, S. Moukouri, D. Rohrlach, A. Mazumdar, S. Bose, C. Henkel, and R. Folman, Realization of a complete Stern-Gerlach interferometer: Towards a test of quantum gravity, *Science Advances* **7**, 1 (2020), arXiv:2011.10928.
- [20] S. MacHluf, Y. Japha, and R. Folman, Coherent Stern-Gerlach momentum splitting on an atom chip, *Nature Communications* **4**, 1 (2013).
- [21] K. Rubin, M. Eminyan, F. Perales, R. Mathevet, K. Brodsky, B. Viaris de Lesegno, J. Reinhardt, M. Boustimi, J. Baudon, J.-C. Karam, and J. Robert, Atom interferometer using two Stern-Gerlach magnets, *Laser Physics Letters* **1**, 184 (2004).
- [22] H. Schmidt-Böcking, A. Templeton, and W. Trageser, eds., *Otto Sterns gesammelte Briefe – Band 2: Sterns wissenschaftliche Arbeiten und zur Geschichte der Nobelpreisvergabe* (Springer, 2019).
- [23] E. Majorana, Atomi orientati in campo magnetico variabile, *Il Nuovo Cimento* **9**, 43 (1932).
- [24] I. I. Rabi, On the process of space quantization, *Phys. Rev.* **49**, 324 (1936).
- [25] O. V. Ivakhnenko, S. N. Shevchenko, and F. Nori, Nonadiabatic Landau-Zener-Stückelberg-Majorana transitions, dynamics, and interference, *Physics Reports* **995**, 1 (2023).
- [26] L. Motz and M. E. Rose, On space quantization in time varying magnetic fields, *Physical Review* **50**, 348 (1936).
- [27] J. Schwinger, On nonadiabatic processes in inhomogeneous fields, *Physical Review* **51**, 648 (1937).
- [28] S. Ashhab, Landau-Zener transitions in an open multi-level quantum system, *Physical Review A* **94**, 1 (2016), arXiv:1609.01150.
- [29] V. N. Ostrovsky and H. Nakamura, Exact analytical solution of the N-level Landau-Zener-type bow-tie model, *Journal of Physics A: Mathematical and General* **30**, 6939 (1997).
- [30] C. E. Carroll and F. T. Hioe, Further generalization of Landau-Zener calculation, *Journal of the Optical Society of America B* **2**, 1355 (1985).
- [31] R. D. Hight, R. T. Robiscoe, and W. R. Thorson, Nonadiabatic spin transitions in an inhomogeneous magnetic field, *Physical Review A* **15**, 1079 (1977).
- [32] L. V. Wang, Multi-stage Stern-Gerlach experiment modeled, *Journal of Physics B: Atomic, Molecular and Optical Physics* **56**, 105001 (2023).
- [33] Z. He, K. Titimbo, D. C. Garrett, S. S. Kahraman, and L. V. Wang, Numerical modeling of the multi-stage Stern-Gerlach experiment by Frisch and Segrè using coquantum dynamics via the Schrödinger equation, *Journal of Physics B: Atomic, Molecular and Optical Physics* **10.1088/1361-6455/acef83** (2023), arXiv:2208.14588.
- [34] K. Titimbo, D. C. Garrett, S. S. Kahraman, Z. He, and L. V. Wang, Numerical modeling of the multi-stage Stern-Gerlach experiment by Frisch and Segrè using coquantum dynamics via the Bloch equation, *Journal of Physics B: Atomic, Molecular and Optical Physics* **56**, 205004 (2023), arXiv:2208.14588.
- [35] J. von Neumann, *Mathematische Grundlagen der Quantenmechanik* (Springer, 1932).
- [36] J. von Neumann, *Mathematical Foundations of Quantum Mechanics*, edited by N. A. Wheeler (Princeton University Press, 2018).
- [37] R. Alicki and M. Fannes, *Quantum Dynamical Systems* (Oxford University Press, 2001).
- [38] F. Benatti, *Dynamics, Information and Complexity in Quantum Systems*, Theoretical and Mathematical Physics (Springer, 2009).
- [39] D. J. Griffiths and D. F. Schroeter, *Introduction to Quantum Mechanics* (Cambridge University Press, 2018).
- [40] E. Arimondo, M. Inguscio, and P. Violino, Experimental determinations of the hyperfine structure in the alkali atoms, *Rev. Mod. Phys.* **49**, 31 (1977).
- [41] M. H. Levitt, *Spin Dynamics: Basics of Nuclear Magnetic Resonance*, 2nd ed. (John Wiley & Sons, 2008).
- [42] R. Schmied, *Using Mathematica for Quantum Mechanics* (Springer, 2020).
- [43] G. Breit and I. I. Rabi, Measurement of nuclear spin, *Phys. Rev.* **38**, 2082 (1931).
- [44] E. Süli and D. F. Mayers, *An Introduction to Numerical Analysis* (Cambridge University Press, 2003).
- [45] J. Bezanson, A. Edelman, S. Karpinski, and V. B. Shah, Julia: A fresh approach to numerical computing, *SIAM Rev.* **59**, 65 (2017).
- [46] E. Fermi, Magnetic moments of atomic nuclei, *Nature* **125**, 16 (1930).
- [47] D. J. Griffiths, Hyperfine splitting in the ground state of hydrogen, *American Journal of Physics* **50**, 698 (1982).
- [48] C. E. Soliveres, The contact hyperfine interaction: An ill-defined problem, *Journal of Physics C: Solid State Physics* **13**, 10.1088/0022-3719/13/34/002 (1980).
- [49] C. Schwartz, Theory of hyperfine structure, *Physical Review* **105**, 173 (1957).
- [50] P. Kusch and V. W. Hughes, *Atomic and Molecular Beam Spectroscopy*, Encyclopedia of Physics / Handbuch der Physik, Vol. 7 / 37 / 1 (Springer Berlin Heidelberg, Berlin, Heidelberg, 1959) pp. 1–172.
- [51] S. S. Kahraman, K. Titimbo, Z. He, and L. V. Wang, Quantum mechanical modeling of the multi-stage Stern-Gerlach experiment conducted by Frisch and Segrè (2022).
- [52] J. D. Jackson, *Classical Electrodynamics*, 3rd ed. (Wiley,

- 1999).
- [53] D. R. Hartree, Results of calculations of atomic wave functions. II.— Results for K^+ and Cs^+ , Proc. R. Soc. Lond. A **143**, 506 (1934).
- [54] H. C. Ohanian, What is spin?, Am. J. Phys. **54**, 500 (1986).
- [55] C. Zener, Non-adiabatic crossing of energy levels, Proceedings of the Royal Society of London. Series A, Continuing Papers of a Mathematical and Physical Character **137**, 696 (1932).
- [56] S. N. Shevchenko, S. Ashhab, and F. Nori, Landau-Zener-Stückelberg interferometry, Physics Reports **492**, 1 (2010), arXiv:0911.1917.
- [57] N. V. Vitanov and B. M. Garraway, Landau-Zener model: Effects of finite coupling duration, Physical Review A **53**, 4288 (1996).